Navigating Solvent Chemistry and Microstructures: Towards Mechanically-enhanced Ceramic-rich Composite Electrolytes

Lingzi Sang[1, 2, *], Mauricio Ponga[3], Michael Fleischauer[4], and Runqi Wu[1]

[1]Department of Chemistry, University of Alberta, Edmonton, Alberta T6G 2G2, Canada

[2]School of Engineering, Faculty of Applied Science, University of British Columbia, Kelowna, British Columbia, V1V 1V7, Canada

[3]Department of Mechanical Engineering, University of British Columbia, Vancouver, British Columbia, V6T 1Z1, Canada

[4] National Research Council, Quantum and Nanotechnologies Research Centre, Edmonton, Alberta T6G 2M9, Canada; Department of Physics, University of Alberta, Edmonton, Alberta T6G 2E1, Canada

Abstract:

Ultra-thin ceramic-rich solid composite electrolytes provide a safer and potentially higher energy-density alternative to liquid electrolytes used in today's lithium-ion batteries. Producing ultra-thin composites with ceramic-like ionic conductivity requires the incorporation of a polymeric binder for enhanced ductility. In this perspective, we discuss two key aspects that must be considered when designing composite electrolytes: (1) the mechanical properties of the composite and its correlation with the ceramic and polymer microstructure, and (2) the chemistry between the ceramic electrolytes, polymers, and solvents used to process the composites. We highlight the importance of understanding (1) the ceramic structure, crystallinity, and particle size upon solvent processing and (2) the ceramic/polymer interface chemistry and its correlation with the microstructure of the composites. We present opportunities in fabricating ultra-thin support structures for composites, optimizing ceramic particle packing parameters, and routes toward mechanically enhanced, compact, composite-based solid-electrolytes.

1. *Introduction*

All-solid-state batteries provide a safer alternative compared to commercial liquid lithium-ion batteries by replacing the flammable, carbonate-based liquid electrolyte with a solid-state ionic conductor. The potentially enhanced energy/power density and improved battery safety are attracting increasing attention for potential applications in electric vehicles, future homes, and grid-scale energy storage systems. Ceramic ion

conductors including sulfides[1-4] (e.g., Li_3PS_4, Na_3PS_4, Li_6PS_5X, $Li_{10}GeP_2S_{12}$, Na_3SbS_4), oxides[5] (e.g., NASICON and garnet), halides[6-11] (e.g., Li_3InCl_6, Li_3ScCl_6, etc.), and their structurally modified derivatives show comparable room-temperature ionic conductivity to liquid electrolytes. However, these solid ceramic ion conductors are mechanically fragile and are typically used in research as millimeter-thick pellets. Reducing the electrolyte thickness to realize high energy/power-density commercial cells requires thinner electrolytes consisting of mechanically enhanced ionic conductors. Besides playing a critical electrochemical role in ion conduction, composite electrolytes are also crucial mechanical elements in an all-solid-state battery configuration. In particular, the composite electrolyte must support mechanical stresses during cell assembly (i.e., tension and initial compressive stack pressure when winding) and lifetime (i.e., variations in stack pressure and bending with electrochemical and thermal cycling). In addition, variations in winding tension or electrode loading, for instance, can lead to subsequent deformation after cycling.[12] Indeed, from a mechanical viewpoint, reducing the thickness of the membrane not only increases the energy density but also promotes the mechanical strength of the all-solid battery because in both cylindrical and pouch cell configurations, electrolyte membranes will likely experience bending stresses due to deformation and in principle, reduced thickness results in smaller strains within the membrane. In a cylindrical cell at a given radius, for instance, the tensile and compressive stress experienced by the surfaces of the electrolyte membrane are directly proportional to its thickness and inversely proportional to the radius of the cylindrical battery. In the particular case of a multicomponent composite electrolyte membrane, changes in the porosity of the inner and outer surfaces might compensate for the accumulated stress, which could in turn affect ionic conductivity.

The overall thickness of an electrolyte composite and its microstructure are among the most important pillars that dictate the mechanical properties of a solid-state composite electrolyte. The goal is to produce thin, high ionic conductivity electrolytes with all the required mechanical properties. Separators for commercial liquid-based lithium-ion batteries are ~20 μm thick; this imposes an upper bound on solid-state electrolyte thickness in order to maintain energy density. This 20 μm cross-sectioning thickness is comparable with the dimensions of the solid-state electrolyte particles. Therefore, to

maintain ceramic-like ionic conductivity and mechanical properties, critical parameters that dictate the ionic transport property should be optimized, this includes particle packing, distribution/size of grains, and the porosity (pore size, geometry, and connectivity) of the overall composite. Composite electrolyte design must balance grain and particle size, morphology, packing, and membrane thickness.

Polymeric binders play a key role in composite electrolyte performance. There are two main configurations; a low-volume percentage polymer acting as a binder of ionically conductive ceramics (**Fig. 1a**) or a high-volume percentage ionic conductive polymer (**Fig. 1b**) with ceramic additives. In the ceramic-rich composite configuration, the ceramic portion exceeds the Li^+ (or Na^+) percolation threshold and the ion transport adopts the same mechanism as the ceramic constituents. The polymer constituents maintain inter-particle contacts but do not provide ion transport pathways. In the ceramic-rich configurations, the activation energy for ion transport (E_a) remains relatively unchanged compared to the pristine ceramic, and E_a is independent of temperature. (**Fig. 1c**) In marked contrast, in polymer-rich electrolytes, ceramic additives are introduced into polymeric ion conductors in order to alter the polymer crystallinity for high ionic conductivity. Specifically, polymer-rich electrolytes provide ionic mobility by associating/dissociating ions with ion affinitive functional groups residing on the polymer backbone, and polymer chain relaxation facilitates ion transport. The activation energy for ionic transport in polymer-rich electrolytes varies with temperature. This temperature-dependency of the activation energy for ion transport is fundamentally limited by the physicochemical properties of polymers (i.e., Li^+ (Na^+) affinity, crystallinity, glass transition temperature, etc.), posing challenges in applications. Wang et al. used $Li_{1.3}Al_{0.}Ti_{1.7}(PO_4)_3$ (LATP) as a plasticizer to reduce the crystallinity of poly(ethylene oxide) (PEO)-based polymer electrolytes. The addition of LATP reduces the glass transition temperature of the PEO-based electrolytes and provides 10^{-3} $mS{\cdot}cm^{-1}$-level ionic conductivity[13], 1-2 orders of magnitude higher compared to solvent-free PEO-based polymer electrolyte. This conductivity was further increased to ~0.1 $mS{\cdot}cm^{-1}$ by tuning the wt% of LATP and compounding a polyimide nanofiber to further reduce the crystallinity of PEO.[14] Yang and co-workers demonstrated that 5 wt% of garnet electrolyte $Li_7La_3Zr_2O_{12}$ (LLZO) and its Ta- or Al-

doped analog functions to modify the local chemical environment of Li^+ in polyacrylonitrile-$LiClO_4$-based polymer electrolyte (PAN-$LiClO_4$). Specifically, a distinct ^6Li chemical environment was found in PAN-$LiClO_4$-LLZO via NMR compared to the ^6Li in either LLZO or PAN-$LiClO_4$. Evidence obtained from an isotope replacement approach indicated that the additives create Li^+ transport pathways across the interface between LLZO and PAN-$LiClO_4$ particles. In this case, the PAN-$LiClO_4$ polymer electrolyte remained amorphous independent of LLZO content, indicating that LLZO was not acting as a plasticizer.[15] By way of contrast, Zheng et al. demonstrated that in a ceramic-rich scenario Li^+ transport adopts a solo pathway – through the LLZO. At a 50 wt% (20 vol%) of LLZO in a PEO-based composite, no Li exchange was found via ^6Li NMR in either the PEO constituents or at the PEO/LLZO interface.[16]

This perspective focuses on the ceramic-rich configuration due to its potential of providing high ionic conductivity, and its relatively polymer-independent ion transport mechanism. In the ceramic-rich configuration, the addition of polymer binders will provide enhanced ductility to the material, however, the reduced ionic conductivity of the composite is expected due to the ion-insulating nature of the binder. In order to achieve minimal polymer binder incorporation for sufficient mechanical property enhancement, it is ideal that polymers are integrated at the ceramic particle, crystal grain, or down to the unit cell level. The microstructures of the composites presumably play key roles in its mechanical properties. In this regard, the volume percentage of the polymer and porosity in the composite will affect the ionic conductivity and the mechanical properties of composite electrolytes. Specifically, porosity will partially compensate for tensile and compressive stresses experienced by the composite during assembly and operation; however, increased porosity will reduce the ionic conductivity of the material by reducing the surface contact between ceramic particles, impacting the cell performance negatively.[17] Compared to weight percentage which is often reported in the discussion of composite electrolytes, the understanding of volume percentage and the specific microstructures are required to access the composite configuration toward the optimal conductivity/ductility combination. Measurements such as electron microscopy and micro-computed tomography can provide insights to access these important morphological characteristics.[18]

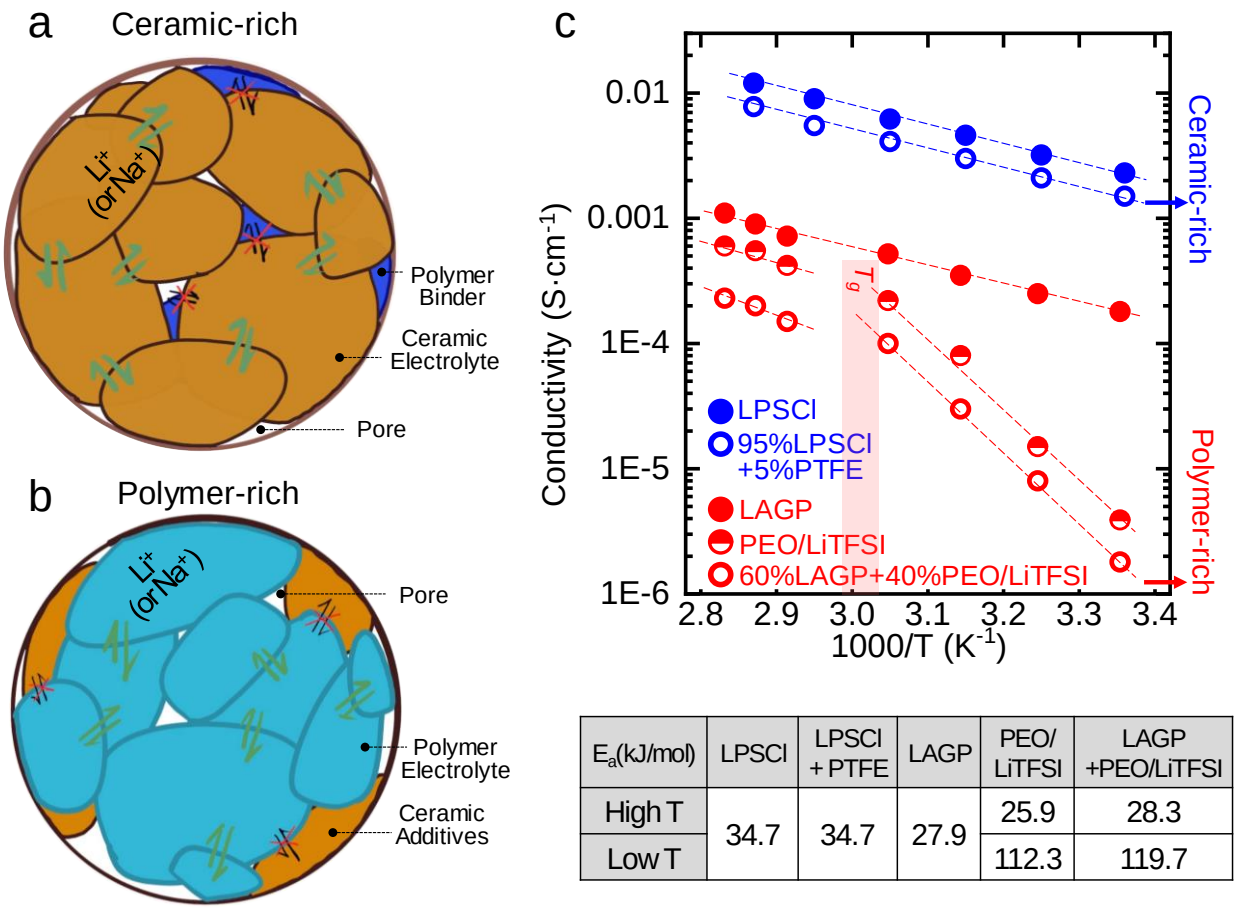

E_a(kJ/mol)	LPSCl	LPSCl + PTFE	LAGP	PEO/ LiTFSI	LAGP +PEO/LiTFSI
High T	34.7	34.7	27.9	25.9	28.3
Low T				112.3	119.7

Figure 1. *(a) Ceramic-rich and (b) Polymer-rich composite electrolytes; (c) Arrhenius plot showing the correlation between ionic conductivity of composites and temperature. Table shows the activation energy of ion transport in the selected composite electrolyte at high and low temperatures. Data used to create the plot and table shown in (c) was extracted from references* [19-24]

Various approaches to integrating ceramic particles and polymer binders have been investigated. These include creating frameworks of ceramics or polymer and incorporating the other components via vacuum or thermal processing, dry mixing ceramic and polymer through a shearing process or mediating polymeric binder and ceramics in a solution followed by casting the slurry to a substrate. Polymer integration can be achieved at the ceramic pellet level. One approach is to synthesize a three-dimensional nanostructural framework of ceramic that serves as the ion transport pathway, within which polymer binder is infiltrated. Bae et al showed a 3D interconnected nanofiller made of $Li_{0.35}La_{0.55}TiO_3$ (LLTO) ceramic electrolyte, and this 3D framework defines the ion percolation pathways within the ceramic component. Polyethylene oxide (PEO) binder was infiltrated into the pores of the 3D structure.[25]

Although the overall thickness of the flexible composite electrolyte was not reported, accounting for the on average 150 nm thick LLTO nanofiller, 100-150 fillers will occupy the cross-section of a 20 µm thick electrolyte. The voids presented in the 3D structure will accommodate mechanically enhancing polymer components. In this previous work, a PEO-based Li^+ conductive polymer was used to fill the pores, and the authors claimed that a second channel for ion transport was provided, the concept remains applicable for the composites fabrication using ion-insulating polymers. This approach requires the formation of a 3D nanostructure of LLTO via a hydrogel matrix. This hydrogel synthetic reaction is specific to LLTO and is so far not applicable to other ceramic electrolytes. In an alternative approach, ceramic electrolytes were infused into an inorganic supporting structure – a 3D ZrO_2 skeleton. Wang and coworkers reported a solution infusion method to embed Li_3InCl_6 into a pre-synthesized ZrO_2 nanowire skeleton.[26] The Li_3InCl_6 constituent provided ion conductive channels. This approach requires solution-synthesized ceramic electrolytes, and the percentage of binder is not tunable. Beyond the infiltration approach, a solvent-free approach was reported and was demonstrated applicable for the synthesis of oxide-, sulfide-, and halide-based composites. Zhang et al.,[27] and Wang et al.[19] both showed shearing mixed ceramic electrolytes with 0.5 wt% of polytetrafluoroethylene (PTFE) binder. The resulting composite shows fiber-like features in the microstructures, supporting the mechanical integrity of a thin and free-standing layer of ceramic. To the best of our knowledge, PTFE is the only dry-processed binder material that has been demonstrated to form fiber-like microstructures providing sufficient mechanical support to the ceramic electrolytes. PTFE, however, is not electrochemically stable at Li^+ and Na^+ reducing potentials[28] and PTFE also undergoes side reactions with cathode materials[29] or graphite anodes[30] during cycling.

The challenge with incorporating binders after the ceramic framework has formed is the need for a driving force for binders to penetrate and fill the voids throughout the ceramic. Another approach is to integrate binders at the single ceramic particle level for designated microstructures that support sufficient mechanical strength. Dong and co-authors show a water-processed composite comprised of 92.5 wt% of Na_3SbS_4 ceramic component and 7.5 wt% of carboxymethylcellulose sodium (CMC-Na) as a binder material. CMC formed a ~50 nm thick coating on the Na_3SbS_4 particles, ca. 0.5%

compared to the particle diameter.[31] The composite provides ceramic Na_3SbS_4-level Na^+ conductivity, and the more than 5-fold decrease of electrolyte thickness provided a 5-fold increase in Na^+ conductance compared to pristine Na_3SbS_4. The unique microstructure formed via solution processing indicates the critical role of solvents – dispersing the ceramic components while defining their particle size, dissolving the binder constituents, and facilitating the formation of coatings. In this case, the surface chemistry between the ceramic particles and the polymer binders facilitates the formation of the unique microstructure.

Ren and co-authors demonstrated the unit cell structural-level integration of polymer binder into sodium thioantimoniate (Na_3SbS_4) ceramic electrolyte by cross-linking the base structure in Na_3SbS_4, the SbS_4^{3-} tetrahedron. Pentaerythritol tetraacrylate (PETEA) was used as the linker.[32] A ceramic-like Na^+ conduction mechanism was observed at temperatures between 17 – 90°C, below the glass transition temperature of the PETEA binder. The activation energy for Na^+ transport within pristine Na_3SbS_4 and its cross-linked analog was demonstrated comparable. This structural-level integration enabled the solution processing of a Na_3SbS_4-based flexible electrolyte membrane. Although not specified in this work, this approach potentially accesses the precise control of binder weight percentage through the specific ceramic-linker reaction chemistry. In this designed chemistry each PETEA monomer exhibits four cross-linking sites, which can potentially host two equivalent Na_3SbS_4 units. Accounting for fully occupied PETEA linkers, composites containing 33 molar% of SbS_4^{3-} can be obtained, approaching the theoretical maximum of ceramic percentage. Tuning the ceramic-to-linker ratio is possible yet requires redesigning the cross-linking chemistry.

2. *Mechanical Properties of Ceramic-rich Composites: Manufactured Configuration and Microstructure*

Substrate-deposited vs. Free-standing Electrolyte

The two major approaches for manufacturing thin composite electrolyte membranes include *substrate deposition* and *free-standing membrane* fabrication. Specifically, substrate-deposited membranes are manufactured over an anode or cathode substrate that acts as a support.[33] The membranes might have a nonwoven network of fibers to

provide mechanical resistance to bending.[33] By contrast, free-standing membranes can be fabricated with or without a support structure. (see **Fig. 2**) To produce free-standing membranes with a support structure, (**Fig. 2a**) various ceramic electrolyte particle types (i.e., nanoparticles,[34, 35] nanorods,[26, 36] or microsized ceramic particles[19, 37]) and polymer components as nanostructures or fibers are mediated in solvents and are subsequently applied via slurry casting[38] or infiltration[25] over the support structure following solvent removal at moderate temperatures in an evacuated environment.[39-41] Woven[38, 39, 42] and nonwoven[40, 41, 43, 44] support structures (**Fig. 2a**) have been used, including cellulose membranes, polymeric net membranes, and glass fibers. These support structures are as thin as 15-30 μm[40] to minimize the overall composite thickness. The support structures also exhibit high porosity (~70%) to accommodate the maximum ceramic electrolyte constituents in the composites.[40] Due to the presence of the ion-insulating polymer constituents, the coverage of ceramic ion conductors is <100%, yet the overall composite shows ceramic-like ionic conductivity – comparable in magnitude (on average 1.6 $mS{\cdot}cm^{-1}$, with a range of 0.18 - 6.31 $mS{\cdot}cm^{-1}$, see **Fig. 2c**), and E_a of ion conduction independent of operating temperature.[19] **(Fig. 1c)** The use of a support structure is shown to resist mechanical failure resulting from loads, providing a robust balance between mechanical flexibility and ionic conductivity; however, the non-zero thickness of the support structure also contributes to additional thickness in the free-standing composite electrolyte. Zhu and coworkers reported that the thicknesses of a cellulose support structure and the composite produced using the support are linearly correlated.[38] This observation is consistent with the generally observed contrast: on average, thicker membranes are produced when a support structure is present (~80 µm) versus absent (~52 µm) as shown in **Fig. 2d**. Significant reductions in thickness are required to meet the target thickness of 20 µm or less.

Overall, free-standing composite electrolytes with no support structure show minimal approachable thicknesses ranging between 15 and 110 μm with an average thickness of 65 µm. (**Fig. 2d**) The diverse manufacturing approaches involve mechanical and chemical processing. To achieve ceramic-like conductivity, a minimal amount of binder was always attempted. For example, the solvent-free processing approach by Wang et al. introduced earlier showed a series of 15 µm thick composites comprised of 0.5 wt%

of PTFE with no support structures.[19] Another approach is to functionalize ceramic electrolyte particles with nanometer-scale homogeneous polymer coatings to improve the adhesion between ceramic particles. Dong et al. showed a solution-processing approach to produce cellulose-encapsulated sodium thioantimonate particles. The less than 10 wt% of cellulose coating provided a ductile interface between particles which enhanced the flexibility of the overall composite.[31] **Fig. 2e** shows the relation between energy density and composite membrane thickness, using data obtained from published information. Although some outliers are present, the data suggested a general trend that thicker membranes result in lower energy-density batteries. The highest 280 $W{\cdot}h{\cdot}kg^{-1}$ energy density was obtained from a free-standing composite electrolyte-based battery.[19] We also note that the subtle differences in computing the mass of the battery (e.g., including the overall mass of electrodes) could lead to discrepancies in the reported values of the energy density.

Particle Packing and Mechanical Loading

Composite electrolyte membranes for mass production require a wide range of mechanical properties. Different requirements will appear depending on the cell type and how the electrolyte is incorporated into the membrane. For instance, in wound cells, rolls of free-standing electrolyte membranes would need sufficient tensile strength, and flexibility to allow cell assembly. Another factor usually overlooked in membrane characterization is Poisson's ratio (ratio of decrease in width to increase in length when under lengthwise tension) of composite membranes.

The specific cell design will impose an overall mechanical load on the cells and determine other specific requirements. For instance, membranes will most likely be subjected to bending stresses, placing requirements on maximal tensile and compressive stresses, membrane porosity, and polymer distribution. Other aspects, such as surface roughness and membrane deformation, must be considered to ensure optimal electrode contact and improve cell rate capability.

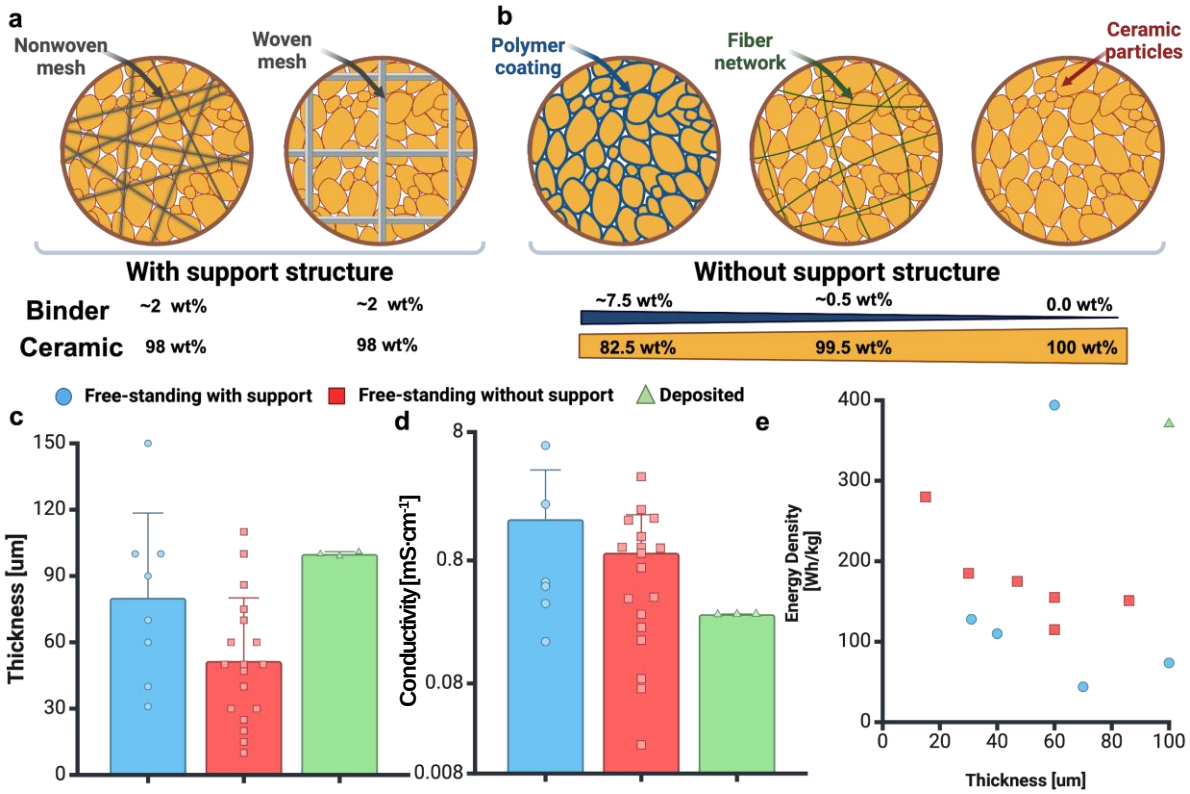

Figure 2. Schematic illustration of free-standing composite solid electrolyte membranes. Free-standing membranes with support structures with high-content ceramic particles (98 wt%) and little binder (2 wt%) for woven and nonwoven structures. Free-standing membranes without support structures showcase a range of binder/ceramic particles from 0.5 wt% to 20 wt% of binder and up to 99.5 wt% of ceramic particles. Solid electrolyte thicknesses and ionic conductivity comparison for different types of membranes. *Data used to create the plot shown in c-e were extracted from references* [18, 19, 25-27, 31, 33, 34, 36-61]

Composite electrolyte membranes have shown a wide range of mechanical properties. In practice, measuring the elastic modulus of a composite electrolyte membrane is challenging due to inaccuracies in determining the end of the elastic regime and the low stiffness of the membranes. Zhu et al. and Kang et al. highlighted high tensile strength ranging from 10 – 20 MPa when support structures were used to manufacture the membranes.[38, 42] Other methods of determining membrane flexibility can be applied, such as the mandril bend test,[62] providing a fast and quantitative comparison between different membranes. The advantage of using these types of tests is the reproducibility of the results, their easy implementation, and the ease of quantitative comparison between different membranes containing multiple types of ceramic particles that might affect the tensile strength of the membrane.

When manufacturing composite electrolyte-based batteries, the ceramic particle size and the compressive load applied to the cell configuration play key roles in the mechanical strength and the ultimate thickness of a battery. The current literature shows that monodispersed particles with an average diameter of 1-5 μm were used in the composites.[19, 25] Some exceptions appeared, including the use of smaller particle sizes between ~50 – 500 nm and nanorods with ~40 nm diameter.[36] The collective results show no obvious correlation between the particle size, morphology, distribution, and the ultimate obtainable membrane thickness. For instance, smaller particle sizes did not result in smaller thicknesses or higher ionic conductivities.[26] Although not investigated extensively, experimental results do show that particle morphology is associated with the ionic conductivity of ceramic electrolytes.[63] Maximized contact areas between ceramic particles will plausibly provide increased ion transport pathways and reduce ion-insulating voids. At the microscopic level, monodispersed ceramic particles will result in high porosities of membranes regardless of binder/solvent and compression methods. The fact that particle size and distribution are relatively independent of key mechanical properties suggests that it is possible to engineer polydispersed particle distribution toward reduced porosity within the composite membrane, enhanced inter-particle contact, increased ionic conductivity, and mechanical properties. Perfect packing of monodisperse spheres in a face-centered cubic structure gives a packing fraction of 74% (26% pore space) based on geometric consideration. Farr and coworkers have shown that for a monodisperse particle distribution, random close-packing, like encountered after tapping a vial of particles, leads to a packing fraction of ~64% (36% void space). In contrast, polydisperse distributions could reach packing factors above 80%.[64] Shimamoto et al. demonstrated that increased packing factors will increase contact points, potentially enhancing the diffusion pathways of ions through the membrane.[65]

Compressive loads are frequently applied to densify composite electrolyte materials, reduce membrane thickness, and improve electrode/electrolyte contacts. Compressive stresses ranging from 30 - 440 MPa have been applied to achieve better contact between anode/cathode and solid electrolytes.[26, 38, 42, 53, 55, 58-60, 63] Aside from the aforementioned benefits, this compressive stress potentially induces plastic deformation

within the composite electrolytes along with creep deformation in lithium electrodes.[66] Although generally unreported, some studies show that the surface roughness of electrolyte membranes ranges between ±0.5 – 1.2 μm.[37] Under compressive loads, the increased interface contact area is likely to induce mechanical deformation within the compliant electrolyte membranes. Practical design could include packaging that produces compressive or bending stresses to ensure proper contact between these components.[65] For instance, vacuum packaging of an all-solid-state battery pack could offer opportunities for applying compressive loads between the components.

3. Ceramic in Solvents: The Evolving Structure and Morphology

Beyond the consideration of composition and mechanical properties, solvents are often involved in the processing of composite electrolytes. Solvents function to mediate the ceramic electrolyte particles with polymeric binders by dissolving the polymeric binder materials yet not chemically reacting with the ceramic electrolytes. Sulfide- and halide ceramic ion conductors are among the most ionically conductive solid-state electrolytes, making them an ideal choice for the ceramic component in solid-state composite electrolytes. However, most sulfides and halides show poor chemical stability in water, oxygen, and polar solvents, posing challenges in solvent-assisted composite synthesis. To achieve ceramic-binder incorporation that provides ceramic-like conductivity and enhanced mechanical properties, a complete set of fundamental understanding of sulfide (halide) – solvent reaction chemistry is required to support the design of composite synthesis.

Halides in Solvent – Dissolution-driven Degradation

Halide Li^+ (Na^+) conductors are comprised of (post-) transition metal (Zr, Y, Sc, In) or lanthanide (Er and Yb) centered octahedrons that adopt an overall layered structure. Li^+ (or Na^+) sites are present between the layers, enabling ion mobility. Halogen ions (F^-, Cl^-, Br^-, I^-) exhibit lower charge density compared to sulfide (S^{2-}), and it was believed that weaker interactions between halogen ions and Li^+ (or Na^+) are present which potentially provide higher Li^+ (or Na^+) conductivity in halide compared to sulfide.[7] Many Li-containing Halide conductors showed a promising liquid-electrolyte-level ionic conductivity;[7, 9, 67, 68] in contrast, the conductivity observed in Na-containing Halide

are two orders of magnitude lower. This observation was attributed to an alternative Na^+ migration behavior due to the larger ionic radius of Na^+.[69] The ionic conductivity of halides shows a strong correlation with their crystal structures.[7, 9, 67-69] Li_3YCl_6 in its crystallized trigonal form shows moderate room temperature conductivity at 4×10^{-5} $S\cdot cm^{-1}$, and its amorphous form exhibits ten times higher ionic conductivity, up to 5.1×10^{-4} $S\cdot cm^{-1}$. Trigonal Li_3ErCl_6 produced by ball milling has a conductivity of 3.3×10^{-4} $S\cdot cm^{-1}$, however through annealing this conductivity reduces to 5.0×10^{-5} $S\cdot cm^{-1}$.[7] In both Li_3YCl_6 and Li_3ErCl_6, when Zr was introduced to the structure to partially replace the center metal, a trigonal-to-orthorhombic structural transition occur resulting along with a Li^+ conductivity increase. This conductivity increase was attributed to the reduced activation energy for Li^+ transport through a different pathway due to the structural transition.[7, 68] Monoclinic halides such as Li_3InCl_6[67] and Li_3YX_6[70] are another type of extensively studied halide ionic conductors. Similar correlation between the crystal structure and the ionic conductivity monoclinic halides were reported. For instance, Schlem et al. demonstrated a strong correlation between the crystal structure of Li_3YX_6 and the Li diffusion mechanism within the material. The slight tweak in the volume of YX_6^{3-} octahedral can induce local structural disorder and alter the thermal displacement of lithium in its designated crystal plane,[70] thus changing the Li^+ mobility in the structure. This octahedral volume and the Li occupancy – another determining factor of the overall ionic conductivity – are directly related to methods used to process Li_3YX_6. Samples synthesized via calcination versus mechanochemical provide discrepancies of both octahedral volume and Li occupancy.[70]

When interacting with solvent, the crystal structures, polyhedral volume, and Li occupancy can plausibly change. This solvent-induced decomposition depends on the nature of solvent–halide interactions. Shen et al. treated Li_3YBr_6 with a range of solvents and interrogated the recovery of halides after post-solvent evaporation. Non-polar solvents including cyclohexane, heptane, hexane, toluene, and xylene show little effect on the Li^+ conductivity of the recovered material. When interacting with polar solvents, Li_3YBr_6 either irreversibly dissolved (i.e., in acetonitrile, N-Methyl-2-pyrrolidone, methyl ethyl ketone, and 1-butanol) or decomposed to form the precursor compounds, LiCl and YCl_6 (i.e., in dimethylformamide, dimethylsulfoxide, and cyclohexanone).[53] Consistently,

in the fabrication of a Li_3InCl_6-ethyl cellulose composite using acetonitrile as the mediation solvent, Li_3InCl_6 was suspected to present in the form of a Li_3InCl_6-acetonitrile complex after solvent removal, also indicating a strong ionic-polar interaction between halide particles and the polar solvent.[51]

Water as a polar protic solvent and its interactions with halide electrolytes are the most extensively studied. Halide electrolytes were found to decompose to LiCl (NaCl) and MCl_x when exposed to moisture, generally irreversibly. Zhu and co-workers calculated the hydrolysis of ternary halide solid-electrolytes Li-M-Cl and Na-M-Cl and considered the formation energy of hydroxides and oxides after H_2O removal. Results suggest that the oxidation of binary halides exhibits positive Gibbs free energies, indicating that the binary halides are the most plausible water-induced decomposition products of halide electrolytes.[71] Although most halide electrolytes undergo irreversible decomposition in H_2O, in the special case of Li_3InCl_6, the dissolution of Li_3InCl_6 in H_2O produces solvated Li^+, In^{3+}, and Cl^-. The removal of H_2O yields the formation of a relatively stable $Li_3InCl_6{\cdot}2H_2O$ complex, facilitating the reversible recovery of Li_3InCl_6 after complete dehydration.[9, 67] A small percentage of $Li_3InCl_6{\cdot}2H_2O$ can further decompose, producing LiCl and $InCl_3$, which can further undergo hydrolysis to form In_2O_3.[72] Coatings on solid-electrolyte particles were fabricated to reduce the moisture permeability of Li_3InCl_6. This partially reversible hydration was applied to synthesize Li_3InCl_6 composites using various water-mediated approaches. Wang et al. fabricated a thin Li_3InCl_6 membrane by infiltrating an electrospun ZrO_2 skeleton with a Li_3InCl_6 aqueous solution followed by evaporation to remove H_2O.[26] Zhao et al. employed a polar protic co-solvent, 1:1 H_2O/ethanol, to perform the Li_3InCl_6 solution infiltration into a glass fiber and obtained Li_3InCl_6 composites exhibiting 5.4×10^{-4} $S{\cdot}cm^{-1}$ Li^+ conductivity,[44] ~50% of pristine Li_3InCl_6.[67] The reduced conductivity was attributed to the presence of Li^+ insulating constituents (glass fiber) and oxidative decomposition product, In_2O_3.[73]

The decomposition of halides in polar solvents is likely driven by the dissolution of a metal-centered polyhedron into solvated monatomic ions. Non-polar solvents will not induce the dissolution of ionic compounds. Using the Li-conducting halide, Li_3MX_6, as an example, in polar solvents, halides are dissociated to form Li^+ and counter ion MX_6^{3-}

and are solvated. In sequence and depending on the specific polar solvents, MX_6^{3-} likely dissolves further to form solvated monoatomic ions M^{3+}, and X^-. Upon the removal of free solvent using heat and vacuum, binary salts (i.e., LiX (NaX) and MX_x) typically form as decomposition products. Polar aprotic solvents such as acetone,[74, 75] acetonitrile[76, 77] and DMF,[78, 79] can form stable solvation structures with monoatomic ions, and the solvated complex ion likely remains over vacuum/heat treatment after the removal of free-solvent.

Sulfide in Solvents – Polyhedral Decomposition

Sulfide-based solid-state electrolytes, $Li_{11}P_3S_7$ glass ceramics, Li_6PS_5Cl argyrodite, and $Li_{10}GeP_2S_{12}$ in particular, are attracting increasing attention due to their liquid-comparable ionic conductivity. These materials contain similar phosphorus-centered polyhedrons as building blocks. The overall structures exhibit a mixed crystalline/amorphous nature, hosting Li^+ defects and/or interstitial sites for Li^+ mobility. Specifically, $Li_{11}P_3S_7$ contains PS_4^{3-} and $P_2S_7^{4-}$, PS_4^{3-} serves as the building block of Li_6PS_5Cl, and $Li_{10}GeP_2S_{12}$ comprised of PS_4^{3-} and GeS_4^{3-}. The moisture and solvent susceptibility of sulfide electrolytes originate from the decomposition of polyhedral structures. The polyhedron degradation and the consequential destruction of the materials' crystal structures result from the Lewis acid-base-like chemistry between the polyhedral structures and solvent molecules.[80] This mechanism is in marked contrast to the mostly dissolution-driven degradation seen in halide electrolytes.

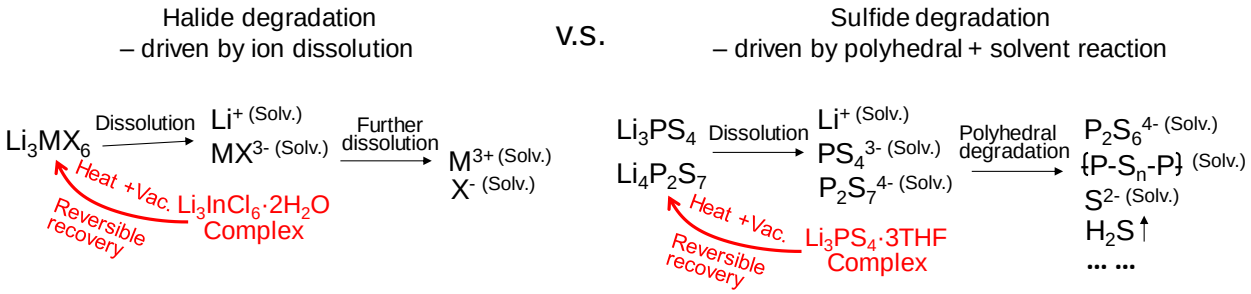

Scheme 1. *Solvent-assisted ceramic electrolyte decomposition – dissolution-driven halide degradation versus sulfide degradation due to polyhedral reaction with solvent molecules. Li-ion conductors are used as examples. Reversible recovery of ceramics occurs when a relatively stable ceramic-solvent complex is formed. Examples of these complexes are $Li_3InCl_6·2H_2O$ and $Li_3PS_4·3THF$.*

$Li_{11}P_3S_7$, Li_6PS_5Cl, and $Li_{10}GeP_2S_{12}$ react with H_2O and form H_2S along with by-products such as lithium binary compounds (LiCl, Li_2S, and Li_3P), phosphate, and germanate. During the reaction, a proton acts as a Lewis acid center and attacks the Lewis-basic sulfur site, extracting sulfur from the PS_4^{3-} and $P_2S_7^{4-}$ polyhedra structures and forming H_2S gas. The oxidation of the phosphorus center likely follows, forming PO_4^{3-}. Beyond H_2O, other proton donors such as methanol and ethanol were reported to react with Li_6PS_5Cl and form H_2S.[63] Nikodimos et al. discussed the moisture susceptibility of sulfide electrolytes and its origin – the Lewis acid-base reaction.[80] In a separate study, a Li_6PS_5Cl complex was synthesized by attaching a weak Lewis acid to the Lewis-basic sulfur site. This complex functions to prevent the proton-sulfur interaction and the irreversible hydrolysis due to the formation of a gaseous H_2S.[81] Other strategies for the suppression of H_2S to reduce the electrolyte decomposition include substituting the P center[82] or introducing additives such as oxides and halides at both the ceramic electrolytes' particle level[83] and structural level.[84-86] These structural designs are intended to reduce the proton affinity of S present in the structures.

Aside from the reaction of S due to its Lewis-basic feature, the P or Ge centers in the polyhedrons exhibit Lewis acidic properties. Electron-donating groups in polar solvents react with P- or Ge-center in PS_4^{3-} or $P_2S_7^{4-}$ and form PS_3^{4-} and $P_2S_6^{4-}$, the building blocks of Li^+ insulators. Tan et al. observed the formation of $P_2S_6^{4-}$ when $Li_7P_3S_{11}$ reacts with acetonitrile and dimethyl carbonate while the structure of $Li_7P_3S_{11}$ remains stable in non-polar solvents such as xylene and toluene.[58] Ruhl and coworkers observed the formation of oligo- and polysulfide in Li_6PS_5Cl treated with THF and acetonitrile. PO_4^{3-} was another by-product following Li_6PS_5Cl – THF reaction. Polar solvents containing proton donors such as ethanol and methanol react with $Li_7P_3S_{11}$ and form Li_2S and P-S_n-P likely accompanying the production of H_2S gas.[63] For LGPS, S_3 radical was found in the suspension of LGPS in polar solvent DMF and NMP. After recovery from DMF and NMP, oxidized Ge was observed in the ceramic electrolyte particle.[59]

Uniquely, THF forms a $Li_3PS_4 \cdot 3THF$ complex when reacting with Li_3PS_4 at room temperature. The complex adopts a different crystal structure compared to β-Li_3PS_4,

and it converts to β-Li_3PS_4 at elevated temperatures. Although THF contains a strong electron-donating site, it does not alter the structure integrity of Li_3PS_4, likely due to the presence of the stable $Li_3PS_4 \cdot 3THF$ complex.[1, 87, 88]

Non-polar solvents were found chemically compatible with $Li_{11}P_3S_7$, Li_6PS_5Cl, and $Li_{10}GeP_2S_{12}$.[58, 60, 63, 87] P-Xylene,[87] toluene,[40, 87] 1,2-dichloroethane,[60] methoxybenzene,[60, 61] and heptane[39, 61] have been applied as mediating solvent to synthesize sulfide composites. Tan et al. calculated the Gibbs free energy of three reactions associated with $Li_3P_7S_{11}$ decomposition: 1) the solvation of $P_2S_7^{4-}$, 2) the reduction of $P_2S_7^{4-}$ forming $P_2S_6^{4-}$ and S^{2-}, and 3) the reaction between $P_2S_7^{4-}$ and PS_4^{3-} forming two equivalent of PS_4^{3-}. No particular correlations were found between the polarity index of a solvent and the Gibbs free energy of all three reactions. This result indicates that the reaction of P and S sites highly depends on the structure of solvents. In particular, the presence and the structure of the Lewis-acidic and Lewis-basic center in the solvent dictate its reaction with sulfide solid electrolyte. Parameters such as formation energy of polyhedra-solvent complexes, electron density (deficiency) of the specific electron donating (accepting) sits, and steric hindrance that can possibly alter the accessibility of the electron-donating (-accepting) sits within the solvent molecule are parameters correlated with the polyhedral decomposition chemistry.

Particle Morphology

Beyond the structural-level decompositions, ceramic particle morphology can alter upon solvent treatment. Ruhl et al. interrogated the reduced ionic conductivity seen in Li_6PS_5Cl following the treatment with three solvents, acetonitrile, THF, and toluene[63]. In all three types of solvent, the crystal structure of Li_6PS_5Cl remains unchanged, however marked differences in Li^+ conductivity were observed from the recovered Li_6PS_5Cl. Within the three solvent-treated samples, toluene-treated Li_6PS_5Cl shows the most significantly reduced Li^+ conductivity, to 0.066 $mS \cdot cm^{-1}$, ca. 25 times lower than the untreated material, although as a non-polar solvent, toluene induces no structural-level decompositions. Electrochemical impedance spectroscopy results suggest an increased capacitance originates from the grain boundary and it is strongly influenced by solvent treatment. For example, acetonitrile treatment induced over one order of magnitude

increase in the grain boundary capacitance in Li_6PS_5Cl, while toluene and THF cause close to two orders of magnitude increase in grain boundary capacitance. At the electrolyte/cathode interfaces, a six-fold increase in interfacial resistance was observed in THF- and toluene-treated Li_6PS_5Cl. The marked change in Li^+ transport properties seen in solvent-treated samples were attributed to the evolved microstructure. Toluene-treated Li_6PS_5Cl shows a continuum of clustered morphology, while acetonitrile- and THF-treated samples show reduced particle size exhibiting more uniform size distribution when compared to pristine Li_6PS_5Cl.

Although the morphological change in ceramic particles is seemingly correlated with the Li^+ transport property within the solid electrolyte, the origin of this possible correlation was unresolved. First, the change in ceramic particle size must originate from the materials' structural-level interaction between the ceramic surface and solvent molecules. In the case that ceramic structure destruction was not observed (i.e., sulfide electrolyte in non-polar solvents) a weak inter-molecular interaction is likely present to partially solvate the ceramic particles, which then followed by a change in particle morphology. It is, therefore, plausible to fine-tune the ceramic particle morphology toward the optimal Li^+ transport property by a selected solvent treatment.

4. Perspectives: A demand for the fundamental understanding of Configuration Engineering, Mechanical Properties, and Solvent-ceramic Chemistries.

Fabricating a solution-processible ceramic-rich composite electrolyte that simultaneously exhibits ceramic electrolyte-like ionic conductivity and sufficient mechanical strength to support a thin and flexible free-standing structure requires a rational design of the composite's microstructure and the processing protocols. To achieve this ultimate goal, a few key fundamental aspects still require in-depth study. This includes the following aspects:

(a) *Ceramic particle size, crystallinity, and local structure*

Understanding the effect of solvent on ceramic particle size, crystallinity, and materials' local structure is important for optimizing the solvent-polymer-ceramic system for composite processing. Yu and coworkers observed a significantly lower Li^+ conductivity across the ceramic/liquid electrolyte interface compared to the conductivity within single

phases. An increased ceramic particle size (i.e., reduced overall interface area) in the liquid electrolyte yielded increased interface Li^+ conductivity, confirming the hypothesis of the high energy barrier for ion transport through the ceramic particle and liquid electrolyte interface.[89] This high energy barrier was attributed to the structural instability at the interface. Busche et al.[90, 91] and Simon et al.[20] combined EIS, ToF SIMS, and XPS to unravel the evolving solid-liquid electrolyte interphase. Schleutker demonstrated Butler-Volmer-like ion transport behavior across the interface and the ion-transfer-driven exchange current across the interface is a function of charge-carrier concentrations.[92] In the similar case of ceramic/polymer composite, reducing the overall interface area is preferred and this can be achieved via increasing ceramic particle size at a designated ceramic wt%. Under this hypothesis, ceramic particles with a diameter close to the thickness (≤100μm) of the composite membrane are seemingly ideal.[89] In ceramic-rich composite electrolytes the crystallinity of the dominating ceramic component dictates the ionic conductivity of the ceramic and the overall composites. The correlation between crystallinity and ionic conductivity varies with the ceramic electrolyte (e.g., higher ionic conductivity was observed in amorphous sulfides and more crystalline Li_3InCl_6). Rigorous grinding and solvent processing are likely playing a key role in introducing amorphousness into the composites. Grinding or solvent treatment, however, is likely to also reduce the particle size, creating an increased interface area. Collectively, insights into the interplay of ceramic particle size and crystallinity in the ionic conductivity of a composite electrolyte are required to guide the design of the material. Also, as indicated in previous studies, defects, and local structures affect the ion transport mechanism.[93] Therefore the effect of solvents and polymer constituents on the local structure of ceramic electrolytes should be interrogated and considered for the selection of the optimal processing approach.

(b) Ceramic–binder reaction and surface chemistry

Interactions between ceramic electrolyte and polymer binders require in-depth analysis. First, possible chemical reaction between selected ceramic and polymer binders are not available. To realize the orthogonal processing of ceramic particle recovery and polymer binder dispersion, the structural integrity of the ceramic and polymer should remain

unchanged throughout the solution process. Second, the distribution of polymer within the composite electrolyte dictates the microstructure of the composite, which impacts the mechanical properties and ionic conductivity[54] of the overall composite. For example, Sakuda et al. examined $Li_{11}P_3S_7$ – based composite prepared in two binder/solvent systems, the styrene butadiene styrene copolymer in methoxybenzene and styrene ethylene butylene styrene in heptane. The former system exhibits less ideal mechanical strength compared to the latter, likely resulting from the different microstructure within the composite.[61] The distribution of polymer is plausibly associated with its dispersion within the ceramic/polymer/solvent slurry. Third, inter-molecular interactions (or the surface/interface energy) between ceramic and polymer will affect the heterogeneity and microstructure of the final composites. For instance, lower interface energy (stronger adhesion) at the particle/polymer interface likely yields polymer coatings on the ceramic particles,[31] in contrast, a higher energy interface likely produces larger domains of polymer segregates dispersed within the overall composite. With the same polymer weight percentage and ceramic particle morphology, the microstructure provided by the unique choice of binder/solvent system will dictate the mechanical properties of the overall composites.

(c) Ultra-thin free-standing membranes

Free-standing membranes present tremendous opportunities for producing miniaturized battery thickness and maximal energy densities. Composite membranes with support structures are generally thicker due to the presence of the support structure. Further reducing the thickness of the composite can benefit from advances in 3D printing techniques to manufacture nano-/microsized support scaffolds to hold slurry mixtures during fabrication. Significant advances in additive manufacturing for nano-architected materials should provide avenues to print support structures with sub-micron resolution.[94, 95] Moreover, the microstructure of free-standing membranes can be further optimized by increasing packing factors using polydisperse ceramic particles. This, in turn, will increase the overall contact area between ceramic particles, ultimately providing more pathways for ion diffusion. At the same time, mechanical loads can also serve as a means to ensure better contact between the different elements in the battery,

and practical design could include packaging that produces compressive or bending stresses to ensure proper contact between these components.

Author Information

Corresponding Author

*Lingzi Sang, lsang@ualberta.ca

Author Contributions

The manuscript was written with the contribution of all authors. All authors have approved the final version of the manuscript. L.S. and R.W. contributed to the discussion of ceramic/solvent chemistry; M.P. and M.F. contributed to the composite mechanical property discussion.

Notes

The authors declare no competing financial interest.

Acknowledgments

L.S. is supported by the Natural Sciences and Engineering Research Council (NSERC) of Canada Discovery program, the Alberta Innovates – NSERC Alliance Advance program, the Canada Foundation for Innovation, and the Government of Alberta, UofA Future Energy Systems. M.P. is supported by the NSERC Discovery program. L.S. and M.P. are supported by and UBC Eminence Program. L.S. and M.F. are supported by the National Research Council Canada, New Beginnings program.

Reference

1. Liu, Z.; Fu, W.; Payzant, E. A.; Yu, X.; Wu, Z.; Dudney, N. J.; Kiggans, J.; Hong, K.; Rondinone, A. J.; Liang, C., Anomalous High Ionic Conductivity of Nanoporous β-Li_3PS_4. *J. Am. Chem. Soc.* **2013,** *135* (3), 975-978.
2. Kato, Y.; Hori, S.; Kanno, R., $Li_{10}GeP_2S_{12}$-Type Superionic Conductors: Synthesis, Structure, and Ionic Transportation. *Adv. Energy Mater.* **2020,** *10* (42), 2002153.
3. Tanibata, N.; Deguchi, M.; Hayashi, A.; Tatsumisago, M., All-Solid-State Na/S Batteries with a Na_3PS_4 Electrolyte Operating at Room Temperature. *Chem. Mater.* **2017,** *29* (12), 5232-5238.
4. Banerjee, A.; Park, K. H.; Heo, J. W.; Nam, Y. J.; Moon, C. K.; Oh, S. M.; Hong, S.-T.; Jung, Y. S., Na3SbS4: A Solution Processable Sodium Superionic Conductor for All-Solid-State Sodium-Ion Batteries. *Angew. Chem. Int. Ed.* **2016,** *55* (33), 9634-9638.

5. Wang, C.; Fu, K.; Kammampata, S. P.; McOwen, D. W.; Samson, A. J.; Zhang, L.; Hitz, G. T.; Nolan, A. M.; Wachsman, E. D.; Mo, Y.; Thangadurai, V.; Hu, L., Garnet-Type Solid-State Electrolytes: Materials, Interfaces, and Batteries. *Chem. Rev.* **2020,** *120* (10), 4257-4300.
6. Wang, Q.; Zhou, Y.; Wang, X.; Guo, H.; Gong, S.; Yao, Z.; Wu, F.; Wang, J.; Ganapathy, S.; Bai, X.; Li, B.; Zhao, C.; Janek, J.; Wagemaker, M., Designing Lithium Halide Solid Electrolytes. *Nat. Commun.* **2024,** *15* (1), 1050.
7. Park, K.-H.; Kaup, K.; Assoud, A.; Zhang, Q.; Wu, X.; Nazar, L. F., High-Voltage Superionic Halide Solid Electrolytes for All-Solid-State Li-Ion Batteries. *ACS Energy Lett.* **2020,** *5* (2), 533-539.
8. Zhou, L.; Zuo, T.-T.; Kwok, C. Y.; Kim, S. Y.; Assoud, A.; Zhang, Q.; Janek, J.; Nazar, L. F., High Areal Capacity, Long Cycle Life 4 V Ceramic All-solid-state Li-ion Batteries Enabled by Chloride Solid Electrolytes. *Nat. Energy* **2022,** *7* (1), 83-93.
9. Li, X.; Liang, J.; Yang, X.; Adair, K. R.; Wang, C.; Zhao, F.; Sun, X., Progress and Perspectives on Halide Lithium Conductors for All-solid-state Lithium Batteries. *Energy Environ. Sci.* **2020,** *13* (5), 1429-1461.
10. Li, X.; Kim, J. T.; Luo, J.; Zhao, C.; Xu, Y.; Mei, T.; Li, R.; Liang, J.; Sun, X., Structural Regulation of Halide Superionic Conductors for All-solid-state Lithium Batteries. *Nat. Commun.* **2024,** *15* (1), 53.
11. Hu, Y.; Fu, J.; Xu, J.; Luo, J.; Zhao, F.; Su, H.; Liu, Y.; Lin, X.; Li, W.; Kim, J. T.; Hao, X.; Yao, X.; Sun, Y.; Ma, J.; Ren, H.; Yang, M.; Huang, Y.; Sun, X., Superionic Amorphous $NaTaCl_6$ Halide Electrolyte for Highly Reversible All-solid-state Na-ion Batteries. *Matter* **2024,** *7* (3), 1018-1034.
12. Bond, T.; Gauthier, R.; Eldesoky, A.; Harlow, J.; Dahn, J. R., In Situ Imaging of Electrode Thickness Growth and Electrolyte Depletion in Single-Crystal vs Polycrystalline LiNixMnyCozO2/Graphite Pouch Cells using Multi-Scale Computed Tomography. *J. Electrochem. Soc.* **2022,** *169* (2), 020501.
13. Wang, Y.-J.; Pan, Y.; Kim, D., Conductivity Studies on Ceramic $Li_{1.3}Al_{0.3}Ti_{1.7}(PO_4)_3$-filled PEO-based Solid Composite Polymer Electrolytes. *J. Power Sources* **2006,** *159* (1), 690-701.
14. He, L.; Liang, W.-H.; Cao, J.-H.; Wu, D.-Y., PI-LATP-PEO Electrolyte with High Safety Performance in Solid-State Lithium Metal Batteries. *ACS Appl. Energy Mater.* **2022,** *5* (4), 5277-5286.
15. Yang, T.; Zheng, J.; Cheng, Q.; Hu, Y.-Y.; Chan, C. K., Composite Polymer Electrolytes with $Li_7La_3Zr_2O_{12}$ Garnet-Type Nanowires as Ceramic Fillers: Mechanism of Conductivity Enhancement and Role of Doping and Morphology. *ACS Appl. Mater. Interfaces* **2017,** *9* (26), 21773-21780.
16. Zheng, J.; Tang, M.; Hu, Y.-Y., Lithium Ion Pathway within $Li_7La_3Zr_2O_{12}$-Polyethylene Oxide Composite Electrolytes. *Angew. Chem. Int. Ed.* **2016,** *55* (40), 12538-12542.
17. Abdollahifar, M.; Cavers, H.; Scheffler, S.; Diener, A.; Lippke, M.; Kwade, A., Insights into Influencing Electrode Calendering on the Battery Performance. *Adv. Energy Mater.* **2023,** *13* (40), 2300973.
18. Cao, D.; Li, Q.; Sun, X.; Wang, Y.; Zhao, X.; Cakmak, E.; Liang, W.; Anderson, A.; Ozcan, S.; Zhu, H., Amphipathic Binder Integrating Ultrathin and Highly

Ion-Conductive Sulfide Membrane for Cell-Level High-Energy-Density All-Solid-State Batteries. *Adv. Mater.* **2021,** *33* (52), 2105505.
19. Wang, C.; Yu, R.; Duan, H.; Lu, Q.; Li, Q.; Adair, K. R.; Bao, D.; Liu, Y.; Yang, R.; Wang, J.; Zhao, S.; Huang, H.; Sun, X., Solvent-Free Approach for Interweaving Freestanding and Ultrathin Inorganic Solid Electrolyte Membranes. *ACS Energy Lett.* **2022,** *7* (1), 410-416.
20. Simon, F. J.; Hanauer, M.; Richter, F. H.; Janek, J., Interphase Formation of PEO20:LiTFSI–Li_6PS_5Cl Composite Electrolytes with Lithium Metal. *ACS Appl. Mater. Interfaces* **2020,** *12* (10), 11713-11723.
21. Kumar, B.; Kumar, J.; Leese, R.; Fellner, J. P.; Rodrigues, S. J.; Abraham, K. M., A Solid-State, Rechargeable, Long Cycle Life Lithium–Air Battery. *J. Electrochem. Soc.* **2010,** *157* (1), A50.
22. Robinson, J. P.; Kichambare, P. D.; Deiner, J. L.; Miller, R.; Rottmayer, M. A.; Koenig Jr, G. M., High Temperature Electrode-electrolyte Interface Formation between $LiMn_{1.5}Ni_{0.5}O_4$ and $Li_{1.4}Al_{0.4}Ge_{1.6}(PO_4)_3$. *J. Am. Ceram. Soc.* **2018,** *101* (3), 1087-1094.
23. Chung, H.; Kang, B., Increase in Grain Boundary Ionic Conductivity of $Li_{1.5}Al_{0.5}Ge_{1.5}(PO_4)_3$ by Adding Excess Lithium. *Solid State Ionics* **2014,** *263*, 125-130.
24. Feng, J. K.; Lu, L.; Lai, M. O., Lithium Storage Capability of Lithium-ion Conductor $Li_{1.5}Al_{0.5}Ge_{1.5}(PO_4)_3$. *J. Alloys Compd.* **2010,** *501* (2), 255-258.
25. Bae, J.; Li, Y.; Zhang, J.; Zhou, X.; Zhao, F.; Shi, Y.; Goodenough, J. B.; Yu, G., A 3D Nanostructured Hydrogel-Framework-Derived High-Performance Composite Polymer Lithium-Ion Electrolyte. *Angew. Chem. Int. Ed.* **2018,** *57* (8), 2096-2100.
26. Wang, S.; Liao, Y.; Li, S.; Cui, C.; Liang, J.; Du, G.; Tong, Z.; Yuan, L.; Zhai, T.; Li, H., Ultrathin All-Inorganic Halide Solid-State Electrolyte Membranes for All-Solid-State Li-Ion Batteries. *Adv. Energy Mater.* **2024,** *14* (6), 2303641.
27. Zhang, Z.; Wu, L.; Zhou, D.; Weng, W.; Yao, X., Flexible Sulfide Electrolyte Thin Membrane with Ultrahigh Ionic Conductivity for All-Solid-State Lithium Batteries. *Nano Lett.* **2021,** *21* (12), 5233-5239.
28. Chakrabarti, N.; Jacobus, J., The Chemical Reduction of Poly(tetrafluoroethylene). *Macromolecules* **1988,** *21* (10), 3011-3014.
29. Tao, R.; Tan, S.; Meyer Iii, H. M.; Sun, X.-G.; Steinhoff, B.; Sardo, K.; Bishtawi, A.; Gibbs, T.; Li, J., Insights into the Chemistry of the Cathodic Electrolyte Interphase for PTFE-Based Dry-Processed Cathodes. *ACS Appl. Mater. Interfaces* **2023,** *15* (34), 40488-40495.
30. Zhang, Y.; Huld, F.; Lu, S.; Jektvik, C.; Lou, F.; Yu, Z., Revisiting Polytetrafluorethylene Binder for Solvent-Free Lithium-Ion Battery Anode Fabrication. *Batteries* **2022,** *8* (6), 57.
31. Dong, S.; Xie, G.; Xu, S.; Tan, X.; Chaudhary, M.; Zhang, Y.; Wu, R.; Wen, F.; Ayranci, C.; Michaelis, V. K.; Quirk, A.; Rosendahl, S. M.; Liu, J.; Fleischauer, M. D.; Sang, L., Cellulose-Encapsulated Composite Electrolyte Design: Toward Chemically and Mechanically Enhanced Solid-Sodium Batteries. *ACS Nano* **2024,** *18* (25), 16285-16296.
32. Ren, Y.; Hortance, N.; McBride, J.; Hatzell, K. B., Sodium–Sulfur Batteries Enabled by a Protected Inorganic/Organic Hybrid Solid Electrolyte. *ACS Energy Lett.* **2021,** *6* (2), 345-353.

33. Xu, R.; Yue, J.; Liu, S.; Tu, J.; Han, F.; Liu, P.; Wang, C., Cathode-Supported All-Solid-State Lithium–Sulfur Batteries with High Cell-Level Energy Density. *ACS Energy Lett.* **2019,** *4* (5), 1073-1079.
34. Li, Z.; Huang, H.-M.; Zhu, J.-K.; Wu, J.-F.; Yang, H.; Wei, L.; Guo, X., Ionic Conduction in Composite Polymer Electrolytes: Case of PEO:Ga-LLZO Composites. *ACS Appl. Mater. Interfaces* **2019,** *11* (1), 784-791.
35. Paolella, A.; Zhu, W.; Xu, G.-L.; La Monaca, A.; Savoie, S.; Girard, G.; Vijh, A.; Demers, H.; Perea, A.; Delaporte, N.; Guerfi, A.; Liu, X.; Ren, Y.; Sun, C.-J.; Lu, J.; Amine, K.; Zaghib, K., Understanding the Reactivity of a Thin $Li_{1.5}Al_{0.5}Ge_{1.5}(PO_4)_3$ Solid-State Electrolyte toward Metallic Lithium Anode. *Adv. Energy Mater.* **2020,** *10* (32), 2001497.
36. Bi, J.; Mu, D.; Wu, B.; Fu, J.; Yang, H.; Mu, G.; Zhang, L.; Wu, F., A Hybrid Solid Electrolyte $Li_{0.33}La_{0.557}TiO_3$/Poly(acylonitrile) Membrane Infiltrated with a Succinonitrile-based Electrolyte for Solid State Lithium-ion Batteries. *J. Mater. Chem. A* **2020,** *8* (2), 706-713.
37. Jin, Y.; Zong, X.; Zhang, X.; Liu, C.; Li, D.; Jia, Z.; Li, G.; Zhou, X.; Wei, J.; Xiong, Y., Interface Regulation Enabling Three-dimensional $Li_{1.3}Al_{0.3}Ti_{1.7}(PO_4)_3$-Reinforced Composite Solid Electrolyte for High-performance Lithium Batteries. *J. Power Sources* **2021,** *501*, 230027.
38. Zhu, G.-L.; Zhao, C.-Z.; Peng, H.-J.; Yuan, H.; Hu, J.-K.; Nan, H.-X.; Lu, Y.; Liu, X.-Y.; Huang, J.-Q.; He, C.; Zhang, J.; Zhang, Q., A Self-Limited Free-Standing Sulfide Electrolyte Thin Film for All-Solid-State Lithium Metal Batteries. *Adv. Funct. Mater.* **2021,** *31* (32), 2101985.
39. Inada, T.; Kobayashi, T.; Sonoyama, N.; Yamada, A.; Kondo, S.; Nagao, M.; Kanno, R., All Solid-state Sheet Battery using Lithium Inorganic Solid Electrolyte, thio-LISICON. *J. Power Sources* **2009,** *194* (2), 1085-1088.
40. Nam, Y. J.; Cho, S.-J.; Oh, D. Y.; Lim, J.-M.; Kim, S. Y.; Song, J. H.; Lee, Y.-G.; Lee, S.-Y.; Jung, Y. S., Bendable and Thin Sulfide Solid Electrolyte Film: A New Electrolyte Opportunity for Free-Standing and Stackable High-Energy All-Solid-State Lithium-Ion Batteries. *Nano Lett.* **2015,** *15* (5), 3317-3323.
41. Zhang, X.; Liu, T.; Zhang, S.; Huang, X.; Xu, B.; Lin, Y.; Xu, B.; Li, L.; Nan, C.-W.; Shen, Y., Synergistic Coupling between Li6.75La3Zr1.75Ta0.25O12 and Poly(vinylidene fluoride) Induces High Ionic Conductivity, Mechanical Strength, and Thermal Stability of Solid Composite Electrolytes. *J. Am. Chem. Soc.* **2017,** *139* (39), 13779-13785.
42. Kang, S. H.; Choi, J.; Kim, J. Y.; Shin, D. O.; Lee, Y.-G.; Lee, J., Mechanically Robust Ultrathin Solid Electrolyte Membranes Using a Porous Net Template for All-Solid-State Batteries. *ACS Appl. Mater. Interfaces* **2023,** *15* (23), 28064-28072.
43. Liu, T.; Zhang, L.; Li, J.; Li, Y.; Lai, K.; Zhang, S.; Zhao, G.; Liu, D.; Xi, Z.; Liu, C.; Ci, L., Sulfide Solid Electrolyte Thin Film with High Ionic Conductive from Slurry-casting Strategy for All-solid-state Lithium Batteries. *J. Electroanal. Chem.* **2023,** *928*, 117032.
44. Zhao, B.; Lu, Y.; Yuan, B.; Wang, Z.; Han, X., Preparation of Free-standing Li_3InCl_6 Solid Electrolytes Film with Infiltration-method Enable Roll-to-roll Manufacture. *Mater. Lett.* **2022,** *310*, 131463.

45. Nam, Y. J.; Oh, D. Y.; Jung, S. H.; Jung, Y. S., Toward Practical All-solid-state Lithium-ion Batteries with High Energy Density and Safety: Comparative Study for Electrodes Fabricated by Dry- and Slurry-mixing Processes. *J. Power Sources* **2018,** *375*, 93-101.
46. Kim, D. H.; Lee, Y.-H.; Song, Y. B.; Kwak, H.; Lee, S.-Y.; Jung, Y. S., Thin and Flexible Solid Electrolyte Membranes with Ultrahigh Thermal Stability Derived from Solution-Processable Li Argyrodites for All-Solid-State Li-Ion Batteries. *ACS Energy Lett.* **2020,** *5* (3), 718-727.
47. Oh, D. Y.; Kim, D. H.; Jung, S. H.; Han, J.-G.; Choi, N.-S.; Jung, Y. S., Single-step Wet-chemical Fabrication of Sheet-type Electrodes from Solid-electrolyte Precursors for All-solid-state Lithium-ion Batteries. *J. Mater. Chem. A* **2017,** *5* (39), 20771-20779.
48. Hippauf, F.; Schumm, B.; Doerfler, S.; Althues, H.; Fujiki, S.; Shiratsuchi, T.; Tsujimura, T.; Aihara, Y.; Kaskel, S., Overcoming Binder Limitations of Sheet-type Solid-State Cathodes Using a Solvent-free Dry-film Approach. *Energy Environ. Sci.* **2019,** *21*, 390-398.
49. Jiang, T.; He, P.; Wang, G.; Shen, Y.; Nan, C.-W.; Fan, L.-Z., Solvent-Free Synthesis of Thin, Flexible, Nonflammable Garnet-Based Composite Solid Electrolyte for All-Solid-State Lithium Batteries. *Adv. Energy Mater.* **2020,** *10* (12), 1903376.
50. Liu, G.; Shi, J.; Zhu, M.; Weng, W.; Shen, L.; Yang, J.; Yao, X., Ultra-thin Free-standing Sulfide Solid Electrolyte Film for Cell-level High Energy Density All-solid-state Lithium Batteries. *Energy Environ. Sci.* **2021,** *38*, 249-254.
51. Mei, H.-x.; Piccardo, P.; Carraro, G.; Smerieri, M.; Spotorno, R., Thin-film Li_3InCl_6 Electrolyte Prepared by Solution Casting Method for All-solid-state Batteries. *J. Energy Storage* **2023,** *72*, 108244.
52. Jiang, Z.; Wang, S.; Chen, X.; Yang, W.; Yao, X.; Hu, X.; Han, Q.; Wang, H., Tape-Casting Li0.34La0.56TiO3 Ceramic Electrolyte Films Permit High Energy Density of Lithium-Metal Batteries. *Adv. Mater.* **2020,** *32* (6), 1906221.
53. Shen, F.; McGahan, M.; Pietras, J. D.; Lau, G. Y.; Doeff, M. M.; Battaglia, V. S.; Tucker, M. C., Tape Casting of Thin Electrolyte and Thick Cathode for Halide-Based All-Solid-State Batteries. *J. Electrochem. Soc.* **2023,** *170* (10), 100505.
54. Riphaus, N.; Strobl, P.; Stiaszny, B.; Zinkevich, T.; Yavuz, M.; Schnell, J.; Indris, S.; Gasteiger, H. A.; Sedlmaier, S. J., Slurry-Based Processing of Solid Electrolytes: A Comparative Binder Study. *J. Electrochem. Soc.* **2018,** *165* (16), A3993.
55. Lee, D. J.; Jang, J.; Lee, J.-P.; Wu, J.; Chen, Y.-T.; Holoubek, J.; Yu, K.; Ham, S.-Y.; Jeon, Y.; Kim, T.-H.; Lee, J. B.; Song, M.-S.; Meng, Y. S.; Chen, Z., Physio-Electrochemically Durable Dry-Processed Solid-State Electrolyte Films for All-Solid-State Batteries. *Adv. Funct. Mater.* **2023,** *33* (28), 2301341.
56. Chen, D.; Hu, C.; Chen, Q.; Xue, G.; Tang, L.; Dong, Q.; Chen, B.; Zhang, F.; Gao, M.; Xu, J.; Shen, Y.; Chen, L., High Ceramic Content Composite Solid-state Electrolyte Films Prepared via a Scalable Solvent-free Process. *Nano Res.* **2023,** *16* (3), 3847-3854.
57. Tron, A.; Hamid, R.; Zhang, N.; Paolella, A.; Wulfert-Holzmann, P.; Kolotygin, V.; López-Aranguren, P.; Beutl, A., Film Processing of Li_6PS_5Cl Electrolyte Using Different Binders and Their Combinations. *J. Energy Storage* **2023,** *66*, 107480.

58. Tan, D. H. S.; Banerjee, A.; Deng, Z.; Wu, E. A.; Nguyen, H.; Doux, J.-M.; Wang, X.; Cheng, J.-h.; Ong, S. P.; Meng, Y. S.; Chen, Z., Enabling Thin and Flexible Solid-State Composite Electrolytes by the Scalable Solution Process. *ACS Appl. Energy Mater.* **2019,** *2* (9), 6542-6550.
59. Wang, X.; Ye, L.; Nan, C.-W.; Li, X., Effect of Solvents on a $Li_{10}GeP_2S_{12}$-Based Composite Electrolyte via Solution Method for Solid-State Battery Applications. *ACS Appl. Mater. Interfaces* **2022,** *14* (41), 46627-46634.
60. Yamamoto, M.; Terauchi, Y.; Sakuda, A.; Takahashi, M., Binder-free Sheet-type All-solid-state Batteries with Enhanced Rate Capabilities and High Energy Densities. *Sci. Rep.* **2018,** *8* (1), 1212.
61. Sakuda, A.; Kuratani, K.; Yamamoto, M.; Takahashi, M.; Takeuchi, T.; Kobayashi, H., All-Solid-State Battery Electrode Sheets Prepared by a Slurry Coating Process. *J. Electrochem. Soc.* **2017,** *164* (12), A2474.
62. Standard Test Methods for Mandrel Bend Test of Attached Organic Coatings. ASTM International: West Conshohocken, PA, United States, 2021; Vol. D522/D522M − 17 (Reapproved 2021), pp 1-5.
63. Ruhl, J.; Riegger, L. M.; Ghidiu, M.; Zeier, W. G., Impact of Solvent Treatment of the Superionic Argyrodite Li_6PS_5Cl on Solid-State Battery Performance. *Adv. Energy Sustainability Res.* **2021,** *2* (2), 2000077.
64. Farr, R. S.; Groot, R. D., Close Packing Density of Polydisperse Hard Spheres. *J. Chem. Phys.* **2009,** *131* (24).
65. Shimamoto, D. S.; Yanagisawa, M., Common Packing Patterns for Jammed Particles of Different Power Size Distributions. *Phys. Rev. Res.* **2023,** *5* (1), L012014.
66. Ding, S.; Fairgrieve-Park, L.; Sendetskyi, O.; Fleischauer, M. D., Compressive Creep Deformation of Lithium Foil at Varied Cell Conditions. *J. Power Sources* **2021,** *488*, 229404.
67. Li, X.; Liang, J.; Luo, J.; Norouzi Banis, M.; Wang, C.; Li, W.; Deng, S.; Yu, C.; Zhao, F.; Hu, Y.; Sham, T.-K.; Zhang, L.; Zhao, S.; Lu, S.; Huang, H.; Li, R.; Adair, K. R.; Sun, X., Air-stable Li_3InCl_6 Electrolyte with High Voltage Compatibility for All-solid-state Batteries. *Energy Environ. Sci.* **2019,** *12* (9), 2665-2671.
68. Kim, S. Y.; Kaup, K.; Park, K.-H.; Assoud, A.; Zhou, L.; Liu, J.; Wu, X.; Nazar, L. F., Lithium Ytterbium-Based Halide Solid Electrolytes for High Voltage All-Solid-State Batteries. *ACS Materials Letters* **2021,** *3* (7), 930-938.
69. Wei, Z.; Nazar, L. F.; Janek, J., Emerging Halide Solid Electrolytes for Sodium Solid-State Batteries: Structure, Conductivity, Paradigm of Applications. *Batteries Supercaps* **2024,** *7* (7), e202400005.
70. Schlem, R.; Banik, A.; Ohno, S.; Suard, E.; Zeier, W. G., Insights into the Lithium Sub-structure of Superionic Conductors Li_3YCl_6 and Li_3YBr_6. *Chem. Mater.* **2021,** *33* (1), 327-337.
71. Zhu, Y.; Mo, Y., Materials Design Principles for Air-Stable Lithium/Sodium Solid Electrolytes. *Angew. Chem. Int. Ed.* **2020,** *59* (40), 17472-17476.
72. Wang, S.; Xu, X.; Cui, C.; Zeng, C.; Liang, J.; Fu, J.; Zhang, R.; Zhai, T.; Li, H., Air Sensitivity and Degradation Evolution of Halide Solid State Electrolytes upon Exposure. *Adv. Funct. Mater.* **2022,** *32* (7), 2108805.
73. Li, W.; Liang, J.; Li, M.; Adair, K. R.; Li, X.; Hu, Y.; Xiao, Q.; Feng, R.; Li, R.; Zhang, L.; Lu, S.; Huang, H.; Zhao, S.; Sham, T.-K.; Sun, X., Unraveling the Origin of

Moisture Stability of Halide Solid-State Electrolytes by In Situ and Operando Synchrotron X-ray Analytical Techniques. *Chem. Mater.* **2020,** *32* (16), 7019-7027.
74. Chen, X.; Li, Z.; Zhao, H.; Li, J.; Li, W.; Han, C.; Zhang, Y.; Lu, L.; Li, J.; Qiu, X., Dominant Solvent-Separated Ion Pairs in Electrolytes Enable Superhigh Conductivity for Fast-Charging and Low-Temperature Lithium Ion Batteries. *ACS Nano* **2024,** *18* (11), 8350-8359.
75. Jarek, R. L.; Miles, T. D.; Trester, M. L.; Denson, S. C.; Shin, S. K., Solvation of Li+ by Acetone, THF, and Diethyl Ether in the Gas Phase and the Ion−Molecule Association Mechanism. *J. Phys. Chem. A* **2000,** *104* (11), 2230-2237.
76. Koo, B.; Hwang, S.; Ahn, K. H.; Lee, C.; Lee, H., Low Solvating Power of Acetonitrile Facilitates Ion Conduction: A Solvation–Conductivity Riddle. *J. Phys. Chem. Lett.* **2024,** *15* (12), 3317-3322.
77. Liu, L.; Shadike, Z.; Cai, X.; Hong, M.; Gao, Y.; Shen, S.; Zhang, J., Regulating the solvation structure of an acetonitrile-based electrolyte for Li/NMC811 batteries cycled at low temperature. *J. Mater. Chem. A* **2024,** *12* (12), 6947-6954.
78. Fujii, K.; Wakamatsu, H.; Todorov, Y.; Yoshimoto, N.; Morita, M., Structural and Electrochemical Properties of Li Ion Solvation Complexes in the Salt-Concentrated Electrolytes Using an Aprotic Donor Solvent, N,N-Dimethylformamide. *J. Phys. Chem. C* **2016,** *120* (31), 17196-17204.
79. Chen, K.; Shen, X.; Luo, L.; Chen, H.; Cao, R.; Feng, X.; Chen, W.; Fang, Y.; Cao, Y., Correlating the Solvating Power of Solvents with the Strength of Ion-Dipole Interaction in Electrolytes of Lithium-ion Batteries. *Angew. Chem. Int. Ed.* **2023,** *62* (47), e202312373.
80. Nikodimos, Y.; Huang, C.-J.; Taklu, B. W.; Su, W.-N.; Hwang, B. J., Chemical Stability of Sulfide Solid-State Electrolytes: Stability Toward Humid Air and Compatibility with Solvents and Binders. *Energy Environ. Sci.* **2022,** *15* (3), 991-1033.
81. Nikodimos, Y.; Jiang, S.-K.; Huang, S.-J.; Taklu, B. W.; Huang, W.-H.; Desta, G. B.; Tekaligne, T. M.; Muche, Z. B.; Lakshmanan, K.; Chang, C.-Y.; Hagos, T. M.; Shitaw, K. N.; Yang, S.-C.; Wu, S.-H.; Su, W.-N.; Hwang, B. J., Moisture Robustness of Li_6PS_5Cl Argyrodite Sulfide Solid Electrolyte Improved by Nano-Level Treatment with Lewis Acid Additives. *ACS Energy Lett.* **2024,** *9* (4), 1844-1852.
82. Kwak, H.; Park, K. H.; Han, D.; Nam, K.-W.; Kim, H.; Jung, Y. S., Li^+ Conduction in Air-stable Sb-Substituted Li_4SnS_4 for All-solid-state Li-Ion Batteries. *J. Power Sources* **2020,** *446*, 227338.
83. Hayashi, A.; Muramatsu, H.; Ohtomo, T.; Hama, S.; Tatsumisago, M., Improvement of Chemical Stability of Li_3PS_4 Glass Electrolytes by Adding M_xO_y (M = Fe, Zn, and Bi) Nanoparticles. *J. Mater. Chem. A* **2013,** *1* (21), 6320-6326.
84. Liu, G.; Xie, D.; Wang, X.; Yao, X.; Chen, S.; Xiao, R.; Li, H.; Xu, X., High Air-stability and Superior Lithium Ion Conduction of $Li_{3+3x}P_{1-x}Zn_xS_{4-x}O_x$ by Aliovalent Substitution of ZnO for All-solid-state Lithium Batteries. *Energy Environ. Sci.* **2019,** *17*, 266-274.
85. Neveu, A.; Pelé, V.; Jordy, C.; Pralong, V., Exploration of Li–P–S–O Composition for Solid-state Electrolyte Materials Discovery. *J. Power Sources* **2020,** *467*, 228250.
86. Ahmad, N.; Zhou, L.; Faheem, M.; Tufail, M. K.; Yang, L.; Chen, R.; Zhou, Y.; Yang, W., Enhanced Air Stability and High Li-Ion Conductivity of

$Li_{6.988}P_{2.994}Nb_{0.2}S_{10.934}O_{0.6}$ Glass–Ceramic Electrolyte for All-Solid-State Lithium–Sulfur Batteries. *ACS Appl. Mater. Interfaces* **2020,** *12* (19), 21548-21558.
87. Lee, K.; Kim, S.; Park, J.; Park, S. H.; Coskun, A.; Jung, D. S.; Cho, W.; Choi, J. W., Selection of Binder and Solvent for Solution-Processed All-Solid-State Battery. *J. Electrochem. Soc.* **2017,** *164* (9), A2075.
88. Gobet, M.; Greenbaum, S.; Sahu, G.; Liang, C., Structural Evolution and Li Dynamics in Nanophase Li_3PS_4 by Solid-State and Pulsed-Field Gradient NMR. *Chem. Mater.* **2014,** *26* (11), 3558-3564.
89. Yu, D.; Tronstad, Z. C.; McCloskey, B. D., Lithium-Ion Transport and Exchange between Phases in a Concentrated Liquid Electrolyte Containing Lithium-Ion-Conducting Inorganic Particles. *ACS Energy Lett.* **2024,** *9* (4), 1717-1724.
90. Busche, M. R.; Drossel, T.; Leichtweiss, T.; Weber, D. A.; Falk, M.; Schneider, M.; Reich, M.-L.; Sommer, H.; Adelhelm, P.; Janek, J., Dynamic Formation of a Solid-liquid Electrolyte Interphase and its Consequences for Hybrid-battery Concepts. *Nat. Chem.* **2016,** *8* (5), 426-434.
91. Busche, M. R.; Weiss, M.; Leichtweiss, T.; Fiedler, C.; Drossel, T.; Geiss, M.; Kronenberger, A.; Weber, D. A.; Janek, J., The Formation of the Solid/Liquid Electrolyte Interphase (SLEI) on NASICON-Type Glass Ceramics and LiPON. *Adv. Mater. Interfaces* **2020,** *7* (19), 2000380.
92. Schleutker, M.; Bahner, J.; Tsai, C.-L.; Stolten, D.; Korte, C., On the Interfacial Charge Transfer between Solid and Liquid Li^+ Electrolytes. *Phys. Chem. Chem. Phys.* **2017,** *19* (39), 26596-26605.
93. Gorai, P.; Famprikis, T.; Singh, B.; Stevanović, V.; Canepa, P., Devil is in the Defects: Electronic Conductivity in Solid Electrolytes. *Chem. Mater.* **2021,** *33* (18), 7484-7498.
94. Vyatskikh, A.; Delalande, S.; Kudo, A.; Zhang, X.; Portela, C. M.; Greer, J. R., Additive Manufacturing of 3D Nano-architected Metals. *Nat. Commun.* **2018,** *9* (1), 593.
95. Hirt, L.; Reiser, A.; Spolenak, R.; Zambelli, T., Additive Manufacturing of Metal Structures at the Micrometer Scale. *Adv. Mater.* **2017,** *29* (17), 1604211.

Biography

Dr. Lingzi Sang is an Assistant Professor at the Department of Chemistry at the University of Alberta. Dr. Sang took her Ph.D. from the University of Arizona (2015) and her BSc. from Xiamen University (2009). Before joining U of A in 2018, Dr. Sang was a postdoctoral research associate at the University of Illinois and Urbana-Champaign. Dr. Sang is broadly interested in chemistry at the interfaces of electrochemical devices such as secondary batteries, fuel cells, and electrochemical sensors. Sang group develops in-operando characterization approaches to correlate the performance of electrochemical devices with the fundamental physiochemical nature of the critical interfaces.

Dr. Mauricio Ponga is an Associate professor at the Department of Mechanical Engineering at the University of British Columbia. Dr. Ponga received his Ph.D. and M.A.Sc. from the University of Seville (Spain) and his bachelors from the National University of La Plata (Argentina). Before joining UBC, Dr. Ponga was a postdoctoral scholar at the California Institute of Technology. Dr. Ponga's research interests focus on modeling and simulating the mechanics of materials at the nanoscale, in particular using atomistic simulation techniques, including ab-initio calculations, molecular dynamics, and coarse-grained simulations for multiscale and multiphysics behavior of materials.

Dr. Michael D. Fleischauer is a Senior Research Officer at the National Research Council Canada's Quantum and Nanotechnologies Research Centre, and an Adjunct professor with the Department of Physics at the University of Alberta. He received his M.Sc. (Physics) and Ph.D. from Dalhousie University. Mike's group focuses on developing and using in-situ and in-operando techniques (electrochemical, structural, and mechanical) to understand and improve energy storage materials in realistic conditions.

Runqi Wu is currently a Ph.D. candidate under the supervision of Prof. Lingzi Sang and Prof. Michael D. Fleischauer at the University of Alberta. She received her B.Sc. degrees from the University of Waterloo and Shandong Normal University in 2021. Her current research focuses on designing and fabricating composite electrolyte membranes for all-solid-state batteries.

ToC Figure